TITLE

The local state of chromatin compaction at transcription start sites controls transcription levels

AUTHORS/AFFILIATIONS

Satoru Ishihara,[1,5,*] Yohei Sasagawa,[2] Takeru Kameda,[2,3] Mana Umeda,[2] Hayato Yamashita,[4] Naoe Kotomura,[1] Masayuki Abe,[4] Yohei Shimono,[1] and Itoshi Nikaido[2,*]

[1]Fujita Health University School of Medicine, Toyoake, Aichi 470-1192, Japan
[2]Laboratory for Bioinformatics Research, RIKEN Center for Biosystems Dynamics Research, Wako, Saitama 351-0198, Japan
[3]Graduate School of Science, Hiroshima University, Higashi-Hiroshima, Hiroshima 739-8526, Japan
[4]Graduate School of Engineering Science, Osaka University, Toyonaka, Osaka 560-8531, Japan
[5]Lead contact
[*]Correspondence: satorui@fujita-hu.ac.jp (S.I.), itoshi.nikaido@riken.jp (I.N.)

SUMMARY

A defined amount of transcript is produced from the transcription start site (TSS) of each gene, suggesting that the binding frequency of RNA polymerase varies among genes. However, what structural feature of the genome controls this frequency remains elusive. We established a method to fractionate chromatin according to its degree of compaction. Histone H3 was evenly detected in open and compact chromatin, but histone H1 was enriched in compact chromatin. Similarly, HP1α and MBD2b were more abundant in compact chromatin, but the levels of tri-methylated H3 (lysine 9) and 5-methyl cytosine subtly increased. Via a genome-wide analysis, nearly the entire genome was found to exist in compact chromatin with no variations between repeat and non-repeat sequences;

however, active TSSs were rarely found in compact chromatin. Based on a correlation between weak compaction and RNA polymerase binding at TSSs, it appears that the local state of chromatin compaction establishes transcription levels.

INTRODUCTION

All physiological reactions on the genomic DNA require the binding of protein factors with various enzymatic activities to the appropriate regions of the genome. However, these reactions occasionally fail when the protein factors cannot access their target regions. In eukaryotic cells in early S-phase, replication is initiated from replication origins within genomic regions where DNA-processing enzymes, such as endonucleases, are able to access the DNA under experimental conditions (Bell et al., 2010; Miotto et al., 2016). Repair and recombination in such enzyme-accessible regions also dominantly occur compared with the levels of these activities in enzyme-inaccessible regions (Adar et al., 2016; Rodgers-Melnick et al., 2016; Marand et al., 2017). Similarly, more abundant transcripts are produced from genes within enzyme-accessible regions (Bell et al., 2011; Cockerill, 2011; Guertin and Lis, 2013). These observations indicate that the accessibility of the genome directly controls the strength of reactions on the genome. Importantly, while replication, repair, and recombination are completed in a single round because of their all-or-nothing output, transcription is a repeated reaction because it is required to synthesize multiple RNA copies. The number of copies is determined by the frequency of the reaction, i.e., the frequency of RNA polymerase binding to the transcription start site (TSS). Therefore, a structure that can vary in its degree of accessibility is required to allow variations of transcription levels.

The chromatin structure largely influences the accessibility of the genome. As the primary structure of chromatin, the genomic DNA is wrapped around a histone octamer to form a nucleosome (Kornberg, 1977). The nucleosomes interact with neighboring nucleosomes and/or non-histone proteins to form a higher-order structure (Woodcock and Ghosh, 2010). Thus, the structures organized in this step-by-step process can hide the genomic DNA

from protein factors and reduce the accessibility of the genome. Via treatment with micrococcal nuclease (MNase), the nucleosome positioning along the genome has been characterized. This investigation revealed that a nucleosome is absent in a region just upstream of the TSSs of actively transcribed genes (Hughes and Rando, 2014). It is widely accepted that such regions, known as nucleosome-depleted regions (NDRs), support RNA polymerase binding (Hughes and Rando, 2014), resulting in a direct correlation between chromatin structure and transcriptional state. However, because this level in the hierarchy of chromatin structure exists in two states, i.e., with or without a nucleosome, the ability to achieve intermediate levels of transcription might not be shown. Although NDRs are more clearly observed at the TSSs of highly transcribed genes via well-positioning of nucleosomes on both sides of the NDR (Teif et al., 2012; Carone et al., 2014; Voong et al., 2016), it has also been reported that the nucleosome positioning around the TSSs of genes that are uniformly transcribed in a given cell population is heterogenous (Small et al., 2014; Lai et al., 2018). In addition to nucleosome positioning, other variables are required in the hierarchy of chromatin structure to allow tuning of the transcription level.

A nucleosome can interact with another nucleosome via the basic tail of histone H4, which has an affinity to an acidic patch on the surface of an adjacent nucleosome (Luger et al., 1997; Kalashnikov et al., 2013). Therefore, an array of multiple nucleosomes, known as “beads on a string”, is often formed via inter-nucleosomal interactions to generate a more compact structure. A 30 nm thick fiber has been historically proposed to represent this more compact structure (Maeshima et al., 2019). Electron microscopy analyses have revealed that *in vitro*-reconstituted nucleosome arrays fold into a 30 nm thick rod-shaped structure that has been conceptualized by two alternative models: a one-start solenoid (Finch and Klug, 1976) or a two-start zigzag (Woodcock et al., 1984). Over the last decade, the results of imaging studies have argued against the existence of the 30-nm fiber and have instead revealed granular structures that are distinct from the rod of the 30-nm fiber (Bouchet-Marquis et al., 2006; Joti et al., 2012; Fussner et al., 2012). Recently, granules of various sizes were observed in nuclei of mouse embryonic stem cells, and these granules were estimated to consist of 4–8 nucleosomes (Ricci et al., 2015). A derivative of the

chromosome conformation capture (3C) method also revealed that motifs consisting of 3–4 nucleosomes were commonly formed in budding yeast (Hsieh et al., 2015). These observations together with live imaging analyses that showed fluctuating movement in individual nucleosomes (Hihara et al., 2012; Nozaki et al., 2013; Ricci et al., 2015; Nozaki et al., 2017) suggest that a static 30-nm fiber structure is unlikely to be formed *in vivo*. How nucleosome arrays are in fact arranged remains under debate; nevertheless, it is not doubted that neighboring nucleosomes are locally compacted. Thus, such a structure must be responsible for regulating the accessibility of the genome, which ultimately controls transcription levels.

In this study, chromatin from cultured cells was successfully fractionated according to its compaction state via sedimentation velocity centrifugation: compact chromatin sedimented into the lower fractions, while open chromatin remained in the upper fractions. Analyses of the fractionated proteins indicated enrichment of HP1α, MBD2b, and histone H1 in the lower fractions, suggesting that these proteins contribute to chromatin compaction. Next-generation sequencing (NGS) of the DNA recovered from each fraction showed that nearly the entire genome was packaged into compact chromatin, with the exception of the chromatin at active TSSs, which was poorly compacted. Because the degree of openness at the TSSs correlated with RNA polymerase binding, the local state of chromatin compaction appears to influence the binding frequency of RNA polymerase, which ultimately regulates the transcription levels of individual genes.

RESULTS

Chromatin was fractionated according to its local compaction state

Chromatin is compacted via direct interactions among neighboring nucleosomes and other chromatin-related proteins. Once chromatin is treated with formaldehyde, such interactions are sufficiently preserved to examine the local state of chromatin compaction. For this study, we chose to use human hepatoma HepG2 cells, for which data on epigenetic marks are available in the ENCODE database (https://www.encodeproject.org/). HepG2 cells were mildly treated with

0.5% formaldehyde. Following solubilization with a detergent, the cells were sonicated to fragment chromatin, resulting in shearing of the genomic DNA into fragments of 300–500 bp on average. Next, the cell extract containing the fragmented chromatin was subjected to ultracentrifugation in a sucrose density gradient to fractionate the chromatin according to the degree of compaction (Hansen, 2002; Gilbert et al., 2004). Following removal of the uppermost layer (Fr-0), five fractions were collected and numbered Fr-1 to Fr-5, from the top to the bottom of the centrifugation tube, respectively (Figure 1A). DNA was purified from each fraction and analyzed by agarose gel electrophoresis (Figure 1B). The DNA appeared as smeared bands in all of the fractions, indicating that the chromatin was distributed throughout the centrifugation tube. Note that the formaldehyde concentration directly influenced the fractional distribution of the chromatin, i.e., when the formaldehyde concentration was reduced, the chromatin tended to remain in the upper fractions, possibly because of weaker preservation of the chromatin compaction (Figure S1). Because the average size of the DNA fragments in Fr-1 to Fr-5 was approximately 300–500 bp (Figure 1B), arrays consisting of a few nucleosomes were mostly distributed in Fr-1 to Fr-5. Next, the proteins in each fraction were recovered by trichloroacetic acid (TCA) precipitation and analyzed by sodium dodecyl sulfate-polyacrylamide gel electrophoresis (SDS-PAGE). After reversal of the crosslinking via incubation at 65°C for 24 hrs, the proteins were loaded into an SDS-PAGE gel (Figure 1C). Fr-1 to Fr-5 contained relatively fewer proteins, although an abundant amount of DNA was detected in Fr-1 to Fr-4 (Figures 1C vs. 1B). To analyze the distributions of core histone H3 and linker histone H1, western blotting experiments with pan antibodies against each histone were performed. The protein preparations were normalized among the fractions based on the amount of DNA. There was slightly less H3 in Fr-1 than in the other fractions, and Fr-2 to Fr-5 contained similar levels of H3, indicating that a comparable number of nucleosomes were incorporated per unit length of DNA (“H3” in Figure 1D and solid line in Figure 1E). H1 was gradually enriched toward Fr-5, and it was estimated that the H1 abundance in Fr-5 was 3.2-fold (1.7 in log2) higher than that in Fr-1, indicating that H1 is involved in the local chromatin compaction (“H1” in Figure 1D and dotted line in Figure 1E).

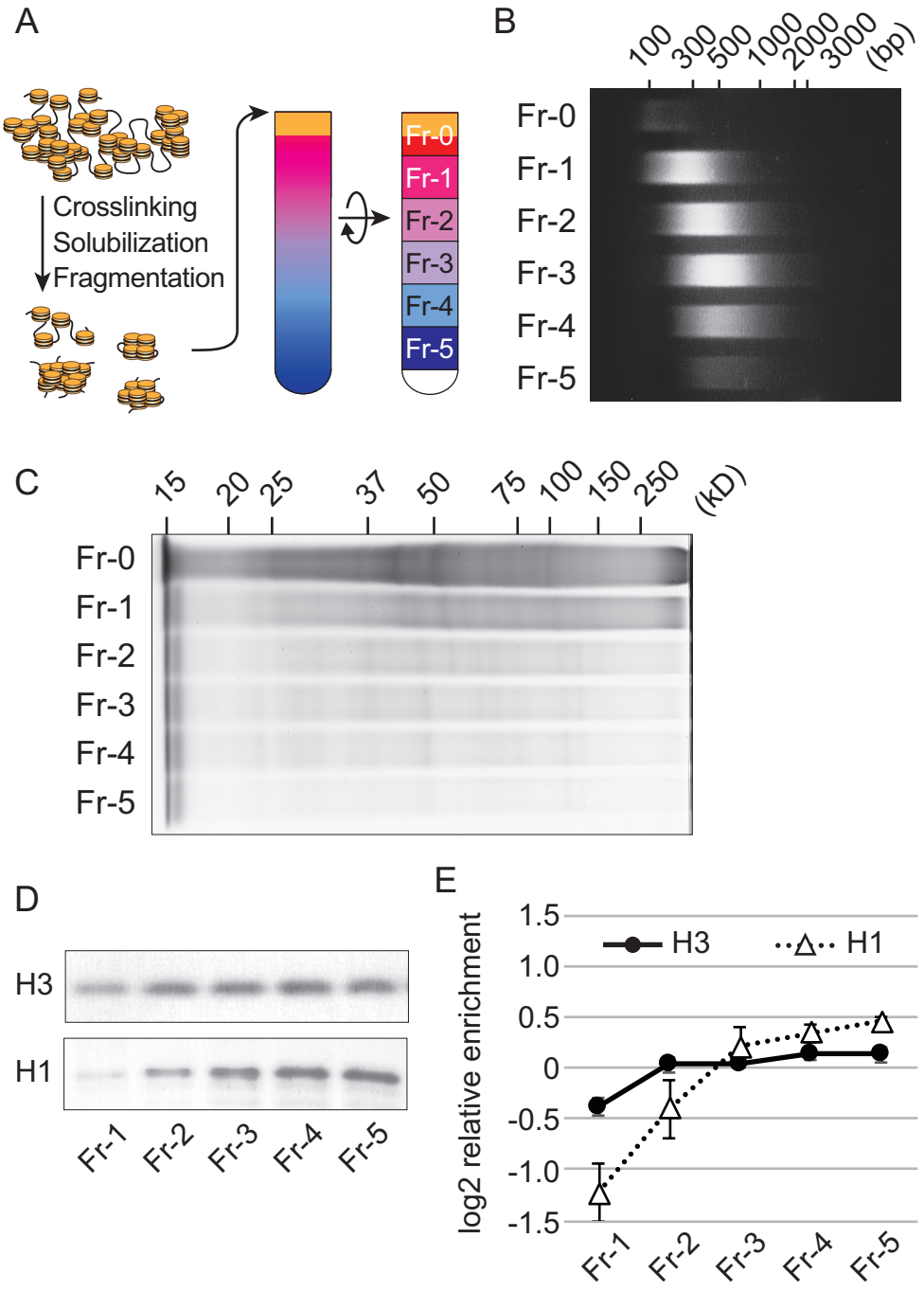

Figure 1. Chromatin fractionation by using sedimentation velocity centrifugation.

(A) A schema of the fractionation method established in this study.

(B) The size distribution of the DNA fragments in the fractionated chromatin. The DNA was size-separated on a 2% agarose gel.

(C) The size distribution of the proteins in the fractionated chromatin. The proteins were size-separated on an 8% SDS-PAGE gel.

(D) Western blotting for histones H3 and H1. The loaded samples were normalized among the fractions based on the amount of DNA.
(E) The fractional distributions of histones H3 and H1. The relative enrichment of the histones in each fraction was calculated from the intensity of the blot signals and is represented by the log2 ratio to the average. Data obtained from at least three independent experiments are represented as the mean ± SD.

Chromatin was prepared from each fraction by immunoprecipitation with a pan anti-histone H3 antibody and then observed via high-speed atomic force microscopy (HS-AFM) (Figure 2A). In Fr-1, objects including histone H3 were unstructured, although some dots did appear to be gathered (arrows in "Fr-1"). On the other hand, bright particles were observed in Fr-2 to Fr-5. Measurement of the particle diameters revealed that the particles became larger toward Fr-5, with the median diameters ranging from 15 nm (Fr-2) to 27 nm (Fr-5) (Figure 2B). Because the length of the fractionated DNA was comparable among the fractions (Figure 1B), the larger particles likely consisted of multiple arrays of nucleosomes and other chromatin-associated proteins. Thus, by using our fractionation method, chromatin was successfully fractionated according to its degree of local compaction.

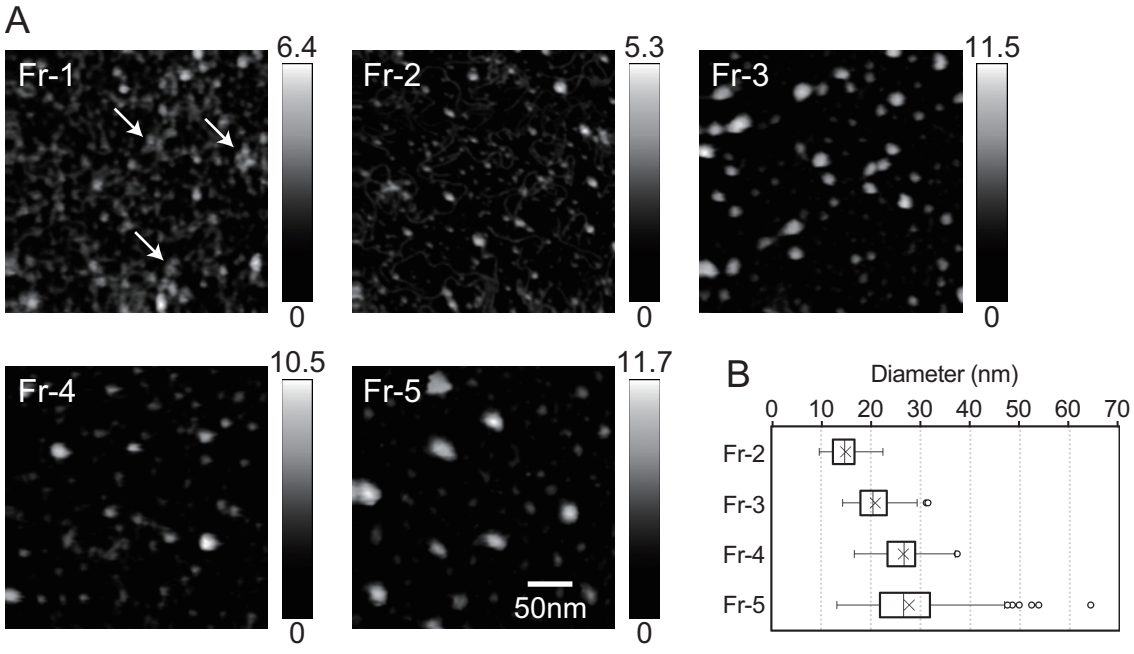

Figure 2. The shape and size of the fractionated chromatin.

(A) HS-AFM images of the fractionated chromatin. Arrows in Fr-1 highlight several dots that are gathered closely. The heights of objects are shown as a grayscale gradation ranging from 0 to a maximum (nm) in each panel. All panels are shown at the same magnification.
(B) The diameters of the chromatin fragments in each fraction. Data were obtained as described in the EXPERIMENTAL PROCEDURES.

The distribution of epigenetic marks and readers in fractionated chromatin

Epigenetic marks are well known to influence chromatin structure. To evaluate the contribution of the marks to the local state of chromatin compaction, we performed immunoblotting analyses to investigate the fractional distribution of histone H3 modified at lysine residues in its amino-terminal tail. The loaded samples were normalized among the fractions based on the amount of DNA. When histone H3 lysine 9 was examined, unmodified and acetylated forms were evenly distributed throughout the fractions (“H3K9un” and “H3K9ac”, respectively, in Figure 3A). On the other hand, tri-methylated H3 at lysine 9 was slightly enriched in Fr-2 to Fr-5 compared with its level in Fr-1 (“H3K9me3” in Figure 3A and solid line in Figure 3C). Similarly, a slight enrichment of tri-methylated H3 at lysine 27 was observed in the lower fractions (“H3K27me3”), but the levels of the unmodified and acetylated forms did not change (“H3K27un” and “H3K27ac”, respectively, in Figure 3A). These observations suggest that methylation of these lysine residues is related to the local chromatin compaction, while acetylation appeared to be independent of the compaction. In addition, when cytosine methylation in CpG dinucleotides was assessed by dot blotting with an anti-5-methyl cytosine antibody, the signals were slightly increased toward Fr-5 (“5meC” in Figure 3A and solid line in Figure 3D). We further investigated the fractional distribution of “readers” of these epigenetic marks. The abundance of HP1α, a reader of H3K9me3, was increased toward Fr-5; however, the abundance of Suz12, a reader of H3K27me3, was decreased toward Fr-5 (“HP1α” and “Suz12” in Figure 3B). These observations indicate that HP1α, but not Suz12, is preferentially present in compact chromatin. When the levels of MBD2 and MeCP2 (5meC readers) were examined, only the abundance of a small variant of MBD2, designated as MBD2b (Wood and Zhou,

2016), was increased toward Fr-5 ("MBD2" and "MeCP2" in Figure 3B). When the distributions of HP1α and MBD2b were compared with those of H3K9me3 and 5meC, respectively, both readers were more highly enriched toward Fr-5 relative to the levels of the epigenetic marks (dotted vs. solid lines in Figures 3C and 3D). These patterns suggest that the readers are only recruited to a fraction of the available epigenetic marks before incorporation into compact chromatin.

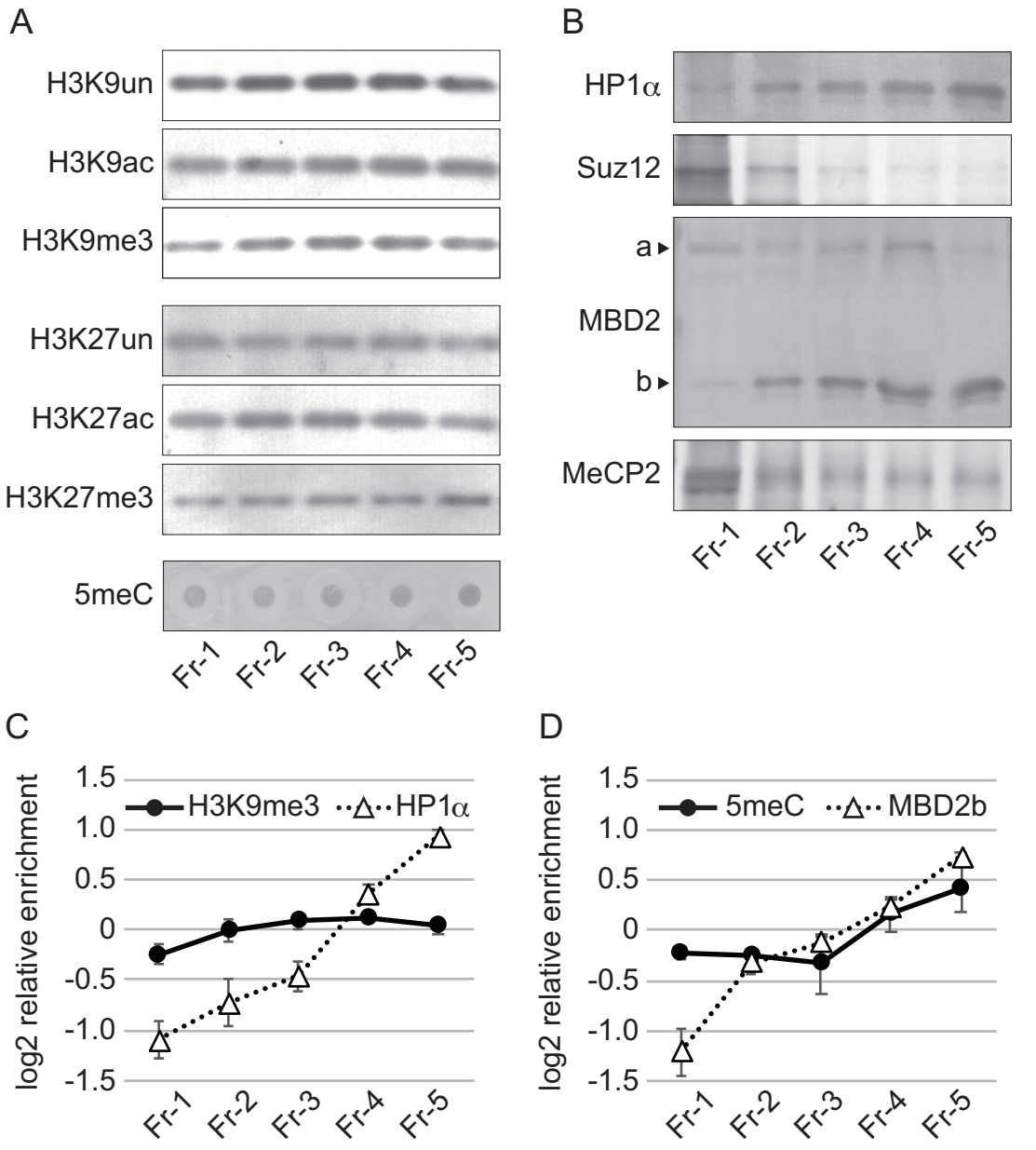

Figure 3. Immunoblot analyses of epigenetic marks and readers in fractionated chromatin.

(A) The fractional distribution of the epigenetic marks was analyzed by western blotting. For 5meC, DNA from the fractionated chromatin was spotted onto a membrane and analyzed by dot blotting.
(B) The fractional distribution of the epigenetic readers was analyzed by western blotting. In the “MBD2” panel, the large and small variants of MBD2 are marked by arrowheads labeled “a” and “b”, respectively.
(C and D) The fractional distributions of the epigenetic marks vs. those of the readers. The relative enrichment of H3K9me3 and HP1α (C), and 5meC and MBD2b (D) was calculated from the intensity of the blot signals and is represented by the log2 ratio to the average. Data obtained from at least three independent experiments are represented as the mean ± SD.

The distributions of active TSSs and repeat sequences in fractionated chromatin

Chromatin at TSSs of highly transcribed genes is opened via nucleosome eviction (Hughes and Rando, 2014), while repeat sequences, such as transposon-derived elements, are mostly packaged into heterochromatin, which is well known to be a compact structure (Saksouk et al., 2015; Iglesias and Moazed, 2017). To investigate how these genomic regions were fractionated by our method, their distributions were assessed using quantitative PCR (qPCR) of DNA recovered from the fractions (Figure 4A). More than 50% of the TSSs for the *GAPDH* and *ACTB* genes, which are abundantly expressed in HepG2 cells, was found in Fr-1, and the proportion gradually deceased toward Fr-5, although 2% of the signal was still detected in Fr-5. As representative repeat sequences, the distributions of *Alu*, L1, and α-satellite sequences were examined by qPCR with primer pairs that annealed to conserved regions in each repeat. The proportions of these repeat sequences in Fr-1 to Fr-3 ranged from 20% to 30%, although they were lower in Fr-4 (12–15%) and Fr-5 (8–9%). These values were quite similar to the proportions of total genomic DNA in the fractions. This similarity is attributable to the fact that almost half of the human genome consists of such repeats. Note that when a different formaldehyde concentration was used, the fractional distributions of the specific genomic regions changed (Figure S2). This outcome mirrors the effect on the distributions of the total genomic

DNA (Figure S1). To simply describe the local state of chromatin compaction, log2 ratios of the proportions in Fr-5 and Fr-1 were calculated ("Fr-5/Fr-1" in Figure 4B). The TSSs of the *GAPDH* and *ACTB* genes showed values of -5.36 and -4.65, respectively, while the values for the repeats and total DNA ranged from -1.79 to -1.25. The apparent differences between the active and repressed reference sequences indicate that the Fr-5/Fr-1 scores are useful for representing the relative levels of the local chromatin compaction.

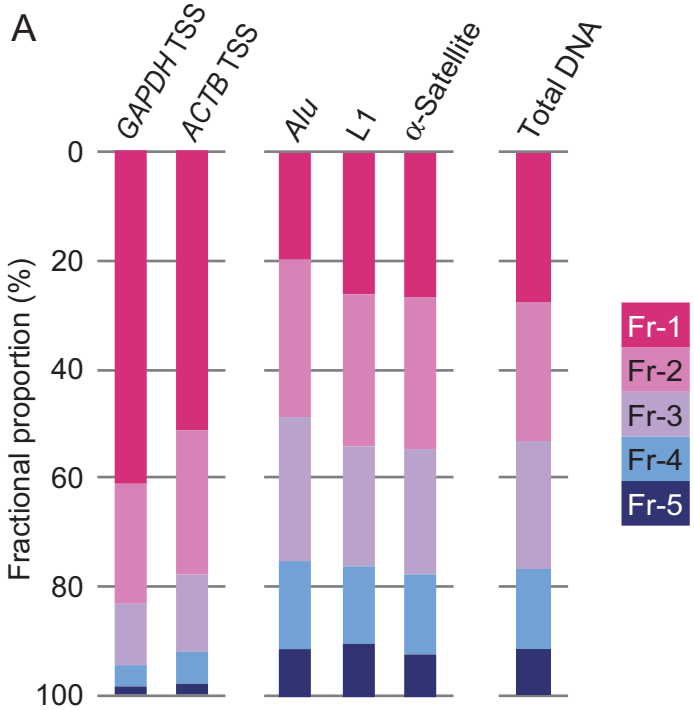

B

	Fr-5 / Fr-1 (log2)
GAPDH TSS	-5.36 ± 0.53
ACTB TSS	-4.65 ± 0.40
Alu	-1.25 ± 0.13
L1	-1.46 ± 0.19
α-Satellite	-1.79 ± 0.09
Total DNA	-1.72 ± 0.23

Figure 4. The fractional proportions of the reference regions in the genome. (A) The TSSs of the *GAPDH* and *ATCB* genes were analyzed to represent active

regions of the genome. *Alu*, L1, and α-Satellite repeat sequences were analyzed to represent repressed regions of the genome. The fractional proportions of the total DNA are also shown.

(B) The proportions (as log2 ratios) of the reference regions described in (A) in Fr-5 to Fr-1. The ratio (designated as "Fr-5/Fr-1") was calculated from data obtained from at least three independent experiments and is represented as the mean ± SD.

Genome-wide features of local chromatin compaction

To elucidate the genome-wide features of local chromatin compaction in HepG2 cells, the DNA in each fraction was analyzed by next-generation sequencing (NGS). Sequence reads were obtained as described in the EXPERIMENTAL PROCEDURES. Approximately 90% of the reads from all of the fractions mapped to the human reference genome hg38 (Figure S3). All of the fractions largely consisted of intergenic and intron regions (Figure S4 and Table S1), although the numbers of reads varied from 6.6×10^7 (Fr-4) to 7.6×10^7 (Fr-2) (Figure S5 and Table S1). Hierarchical cluster analyses were performed to describe the uniqueness of Fr-1 compared with Fr-2 to Fr-5 (Figure S6).

Using a 2,000 kb region of chromosome 14, which consists of a gene-rich region at the center and relatively long intergenic regions on both sides, the local state of chromatin compaction was compared with the levels of epigenetic marks using the Integrative Genomics Viewer (Figure 5A). Fr-5/Fr-1 scores were calculated from the Fr-1 and Fr-5 reads (Tracks 1 and 2, respectively) and were represented as a heatmap (Track 3). The mapped data for 5-methyl cytosine (5meC), DNase hypersensitivity (DHS), and histone modifications (H3K9ac, H3K27ac, H3K9me3, and H3K27me3) in HepG2 cells were obtained from the ENCODE database (accession numbers: GSM2308630, GSM2400286, GSM733638, GSM733743, GSM1003519, and GSM733754, respectively) (Tracks 4 to 9). Transcripts from the HepG2 cells used in this study were also sequenced by NGS (Track 11). As indicated by the blue stripes present in most of Track 3 in Figure 5A, the Fr-5/Fr-1 scores at most of the positions reached nearly -1.0, suggesting that the chromatin across this 2,000 kb region was compacted at a level similar to those of the repeat sequences. While

5meC was restricted in the central gene-rich region (Track 4), H3K9me3 and H3K27me3 were mainly observed outside of the central region (Tracks 8 and 9). These distributions were not correlated to the “blue” regions that indicate compact chromatin (Track 3). Figure 5B shows a magnified view of an 80 kb region from a central part of the 2,000 kb region (red bar in Track 10 of Figure 5A). Three genes, *GEMIN2*, *TRAPPC6B*, and *PNN*, appear (in this order) in the 80 kb region. The *GEMIN2* and *PNN* genes are oriented rightward, while the *TRAPPC6B* gene is oriented leftward (Track 10). As marked with arrows above Track 3 in Figure 5B, three regions with dense red stripes were found, indicating that the chromatin in these regions was poorly compacted. Intriguingly, these regions were located over the TSSs of the three genes (Tracks 3 vs. 10) and corresponded to stretches without 5meC (Tracks 3 vs. 4). These observations suggest that the absence of 5meC might be required for the local openness of chromatin at TSSs. The three regions also corresponded to stretches with DHS (Tracks 3 vs. 5), indicating that the open chromatin can be well digested by DNase I. H3K9ac, H3K27ac, and H3K27me3 were recruited over the TSSs but spread more widely compared with their distributions in the “red” regions (Tracks 3 vs. 6, 7, and 9, respectively). Again, the local chromatin compaction appeared to be distinct from any structures defined by these histone modifications.

The fractional distributions at 18 points (marked with red numbered arrowheads in Track 10 of Figure 5B) were evaluated by qPCR (Figure S7). More than 40% of the TSSs of the three genes was found in Fr-1 (Points 2, 12, and 14), while the proportions of the other points in Fr-1 were less than 30%. The Fr-5/Fr-1 score of each point was calculated (Figure 5C). The score at the *PNN* TSS was -5.12 (Point 14), which was lower than those of the *GEMIN2* TSS (-3.63) and the *TRAPPC6B* TSS (-3.77) (Points 2 and 12, respectively). These scores were inversely correlated to the transcript abundance, as shown in Track 11 in Figure 5B. The regions outside the TSSs showed much higher Fr-5/Fr-1 scores (-2.33 to -1.44) (Figure 5C), which were comparable to the scores of the repeat sequences (Figure 4B). These results suggest that chromatin is *per se* compacted without making a distinction between repeat and non-repeat sequences, but that the compaction is locally attenuated at the TSSs of active genes.

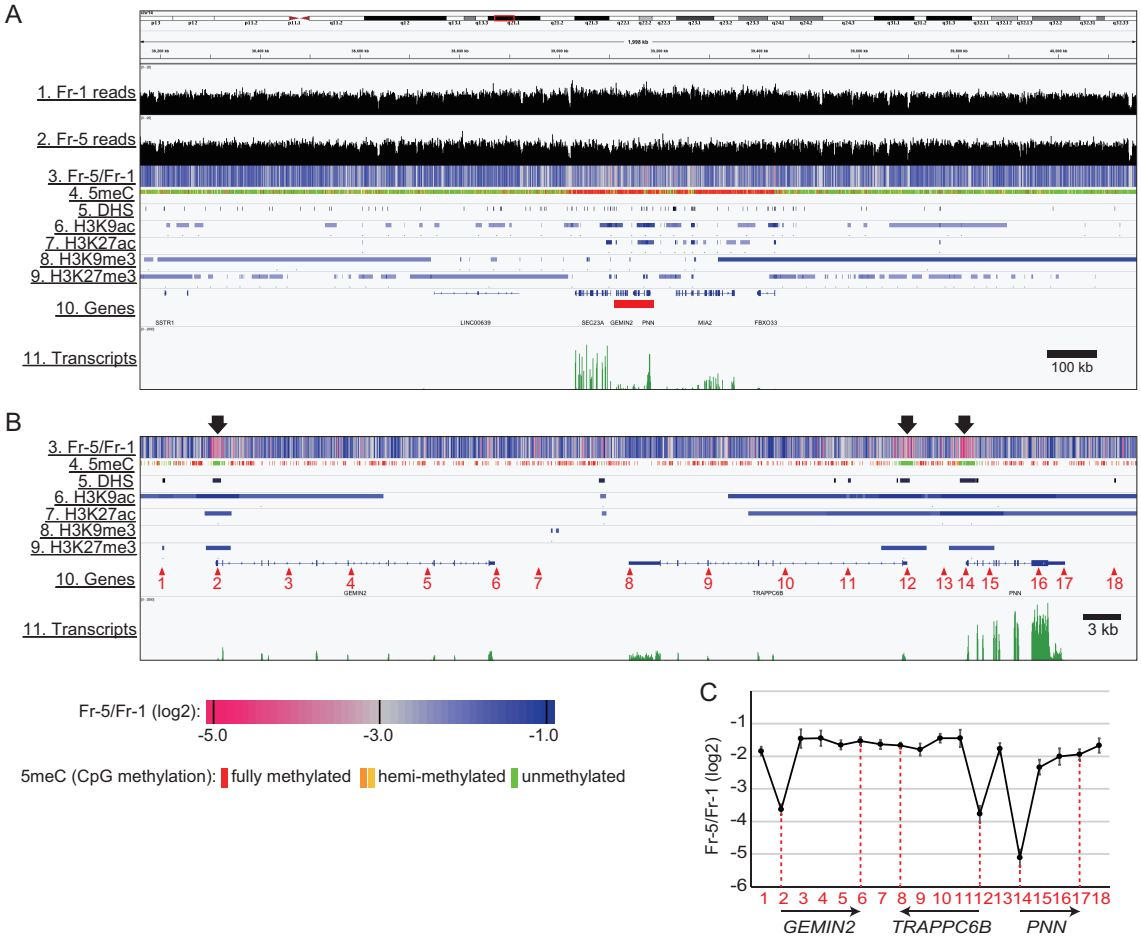

Figure 5. The trimmed landscape of the local chromatin compaction vs. epigenetic marks.

(A) The Fr-5/Fr-1 magnitudes (Track 3), the epigenetic mark distributions (Tracks 4 to 9), and the transcript abundance (Track 11) in a 2,000 kb region of chromosome 14 were visualized via the Integrative Genomics Viewer.

(B) A magnified view of an 80 kb region indicated by a red bar in Track 10 of (A). The chromatin was poorly compacted in the three regions highlighted by the arrows above Track 3.

(C) The Fr-5/Fr-1 scores at the 18 positions indicated by the red numbered arrowheads in Track 10 of (B). Data obtained from at least three independent experiments are represented as the mean ± SD. The positions and orientations of the genes within the 80 kb region are shown with arrows.

We next focused on the bodies of active genes. To clarify the

relationship between transcription level and local chromatin compaction, active genes were categorized into three groups based on their transcription levels, as described in the EXPERIMENTAL PROCEDURES ("Low", "Mid", and "High" in Figure 6A). Nearly the entire gene bodies of the "Low" genes were evenly detected in all of the fractions, while only the TSSs were more abundant in Fr-1 and less abundant in Fr-5. This pattern was also observed for the "Mid" genes. Importantly, the Fr-1-biased distribution of the "Mid" TSSs was more apparent than that of the "Low" TSSs, suggesting a correlation between the compaction at the TSS and the transcription level. On the other hand, for "High" genes, the entire bodies were largely detected in Fr-1, suggesting that openness of the chromatin across the gene body is required for a high level of transcription. Intriguingly, the transcription end sites (TESs) of the "High" genes were slightly less abundant in Fr-1 compared with the levels of the other parts of the gene bodies. Thus, moderate compaction of the TESs may be part of the transcription termination mechanism for the "High" genes. The Fr-5/Fr-1 scores of the TSS and TES of each gene were calculated and plotted on a scatter diagram against the transcription level (Figure 6B). The downward slopes of the approximation lines for both sites indicated an inverse correlation between the Fr-5/Fr-1 scores and the transcription levels. The slope of the TSS line was steeper than that of the TES line, indicating that the correlation of the TSSs was stronger than that of the TESs. To search for a correlation between the compaction at the TSS and RNA polymerase II (Pol II) binding, data from a chromatin immunoprecipitation-sequencing (ChIP-Seq) experiment for Pol II in HepG2 cells were obtained from the Gene Expression Omnibus (GEO) database (accession number: GSM2864932). Expectedly, the binding level of Pol II peaked at the TSSs, and the peak heights were reflected in the transcription levels (Figure S8). In a scatter diagram of the Pol II binding levels against the Fr-5/Fr-1 scores at the TSSs, an inverse correlation was observed (Figure 7A), indicating that Pol II binds less frequently to TSSs in chromatin with higher Fr-5/Fr-1 scores. Taken together, these results suggest that local chromatin compaction, particularly at TSSs, can attenuate transcription possibly by reducing the binding frequency of RNA Pol II.

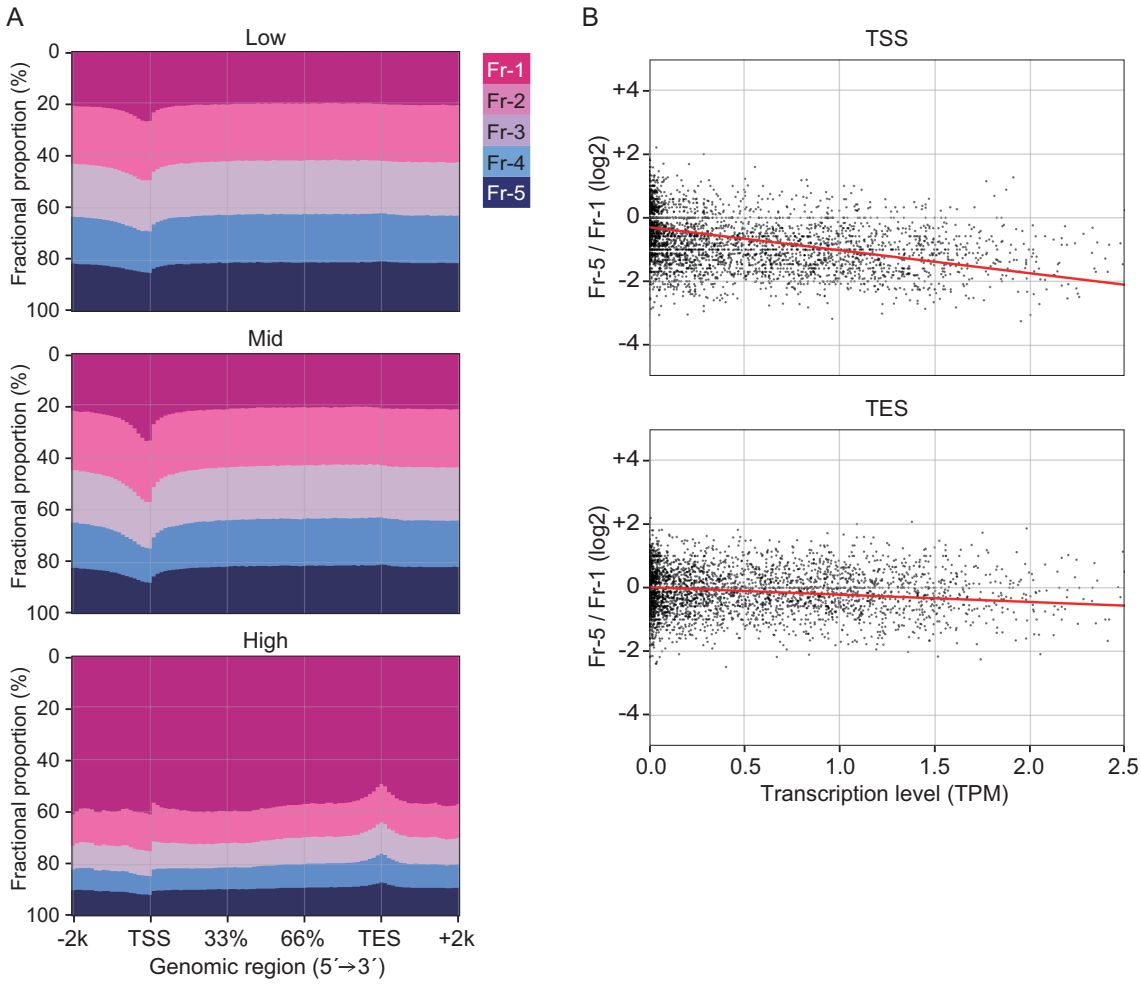

Figure 6. The correlation between the local state of chromatin compaction within the gene body and the transcription level.

(A) The fractional proportions from 2 kb upstream of the TSSs to 2 kb downstream of the TESs of active genes. The genes were divided into three groups based on their transcription levels: “Low”, “Mid”, and “High” (see the EXPERIMENTAL PROCEDURES).

(B) Scatter diagrams comparing the transcription levels (as log_10(TPM + 1)) and the Fr-5/Fr-1 scores at the TSSs or TESs of active genes. The red line in each panel represents an approximation line of the scatter points (see the EXPERIMENTAL PROCEDURES). Data for each gene are listed in Table S2.

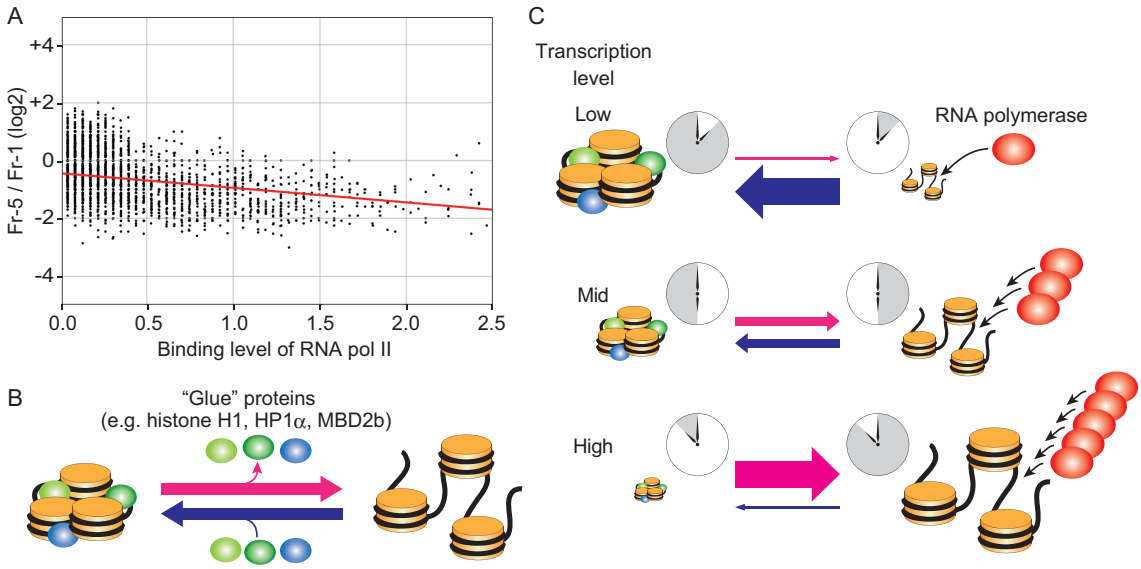

Figure 7. A model of the quantitative regulation of transcription by the local state of chromatin compaction.

(A) A scatter diagram comparing the RNA Pol II binding levels and the Fr-5/Fr-1 scores at the TSSs. The red line represents an approximation line of the scatter points (see the EXPERIMENTAL PROCEDURES).

(B) Chromatin with a few nucleosomes (three in this figure) is locally compacted and opened in equilibrium. When histone H1, HP1α, and/or MBD2b are incorporated into chromatin as "glue" (green ellipses), chromatin is preferentially compacted.

(C) The transcription level is regulated by the equilibrium in the local chromatin compaction, which affects the binding frequency of RNA polymerase (red ellipses). When the equilibrium is biased toward the compact state, the time window for RNA polymerase binding is shortened (in "Low" transcription). Conversely, a bias toward the open state widens the time window for RNA polymerase binding (in "High" transcription). A middle length of the time window leads to "Mid" transcription.

DISCUSSION

In the field of chromatin biology, the positioning of nucleosomes, which consist of approximately 147 bp of DNA, has been well characterized by NGS combined

with MNase treatment (Schones et al., 2008; Voong et al., 2017). Furthermore, an advanced 3C method, i.e., Hi-C, revealed the existence of a topologically associating domain (TAD) that includes a megabase-scaled DNA element (Lieberman-Aiden et al., 2009; Sexton et al. 2012; Dixon et al., 2012; Nora et al., 2012). Based on the data gathered using the novel approach we established in this study, we propose that local chromatin compaction represents another level in the hierarchy of chromatin structure.

DNA-processing enzymes, e.g., endonuclease or transposase, have been historically used to analyze chromatin structure (Tsompana and Buck, 2014). This type of analysis is based on whether the enzyme can access and then digest (or recombine with a probe sequence) the linker DNA between nucleosomes. Thus, these approaches are based on the accessibility rather than the inaccessibility of chromatin. However, in chromatin compacted within the narrow space of a few nucleosomes, the linker DNA may not be hidden among the nucleosomes, and it may be accessible to the enzymes that are smaller than the RNA polymerase complex (Maeshima et al., 2015). It has been reported that endonucleases such as MNase and *Alu*I restriction enzyme can equally digest genomic DNA in open and compact chromatin, although low concentrations of such enzymes are useful for identifying hyper-accessible regions (Schwartz et al. 2019; Chereji et al. 2019). These enzyme-based methods do not seem to be sufficient for determining whether chromatin is locally compacted or not. In this study, to simultaneously evaluate the accessibility and inaccessibility of chromatin, a strategy was designed to biochemically separate open and compact chromatin via fractionation by ultracentrifugation (Figure 1A). As confirmed by the HS-AFM experiments (Figure 2), chromatin was successfully fractionated according to the magnitude of its local compaction.

Considering fluctuating movement of nucleosomes (Hihara et al., 2012; Nozaki et al., 2013; Ricci et al., 2015; Nozaki et al., 2017), chromatin is in equilibrium between moments when neighboring nucleosomes are associated with and dissociated from each other (Figure 7B). Importantly, there is a restricted time window in this equilibrium during which RNA polymerase can access TSSs, suggesting that the length of this window could determine the

binding frequency of RNA polymerase. When the equilibrium is shifted toward compact chromatin, transcription would be attenuated because of less RNA polymerase binding ("Low" in Figure 7C); when the equilibrium is shifted toward open chromatin, transcription would be enhanced because of more RNA polymerase binding ("High" in Figure 7C). When chromatin from a cell population was subjected to this fractionation technique, even highly active TSSs were gradationally distributed toward Fr-1 (Figure 4), indicating that the chromatin at the TSSs is not uniformly opened. In our experiment, the equilibrium would be detected as a mixture of variously compacted structures that were obtained from a snapshot of a cell population. Because the proportion of compact vs. open structures in the mixture is reflected in the Fr-5/Fr-1 score, it would be reasonable to conclude that the Fr-5/Fr-1 score is inversely correlated to the transcription level via changes in the binding frequency of RNA polymerase.

All of the epigenetic marks examined in this study, i.e., H3K9ac, H3K27ac, H3K9me3, H3K27me3, and 5meC, were detected throughout all of the fractions, although their specific fractional distributions varied slightly (Figure 3A). These observations indicate that none of these marks are a direct determinant of whether or not chromatin is compacted. However, considering that HP1α and MBD2b were more abundant toward Fr-5 than were H3K9me3 and 5meC (Figures 3C and 3D), some H3K9me3 and 5meC marks might have served as platforms for HP1α and MBD2b, respectively. Similarly, based on the observation of a clear enrichment of histone H1 toward Fr-5, which was not observed for histone H3 (Figure 1E), it appears that histone H1 was recruited to a limited fraction of the nucleosomes. Thus, HP1α, MBD2b, and histone H1 may all be selectively recruited to their marks. Previous experiments with reconstituted chromatin showed that HP1α bridges two adjacent nucleosomes (Machida et al., 2018), and that histone H1 promotes condensation among three nucleosomes (White et al., 2016). In addition, an *in vivo* imaging study showed that histone H1 is preferentially incorporated into "clutches" of a few nucleosomes (Ricci et al., 2015). Although the structural relationship between MBD2b and nucleosomes remains unclear because MBD2 family protein binds

directly to DNA, it is clear that HP1α and histone H1 operate on a local structure that comprises a few nucleosomes of chromatin. Histone H1 repeatedly associates with and dissociates from chromatin every few minutes (Lever et al., 2000; Misteli et al., 2000). Such dynamic association of histone H1 would be related to chromatin compaction in equilibrium. Together, histone H1, HP1α, and MBD2b could function as “glue” between the adjacent nucleosomes in compact chromatin (Figure 7B).

Heterochromatin and euchromatin, which were originally defined via cytological observations, have been proposed as intranuclear structures that act as a transcriptional switch (Freneter et al., 1963). Furthermore, epigenetic marks have been widely recognized to influence the formation of heterochromatin and euchromatin (Allis and Jenuwein, 2016). Our study has provided evidence of a tendency for the formation of compact vs. open chromatin, which extend over a few nucleosomes. These structures seem to be less temporally and spatially stable relative to heterochromatin and euchromatin. Because a portion of the H3K9me3 and 5meC marks, which are considered heterochromatin marks, were involved in the local chromatin compaction via recruitment of HP1α and MBD2b, respectively, the compact chromatin might be an intermediate structure in the process leading to the formation of typical heterochromatin. Fine-tuning of transcription would be achieved at such a flexible level in the structural hierarchy of chromatin.

ACKNOWLEDGMENTS

We thank Kazuhiro Maeshima for his helpful comments on the manuscript. The antibodies against H3K9un and H3K27un were gifts from the MAB Institute, Inc. We also thank Akihiro Matsushima and Manabu Ishii for their assistance with the infrastructure for the data analyses in the Laboratory for Bioinformatics Research, RIKEN Center for Biosystems Dynamics Research. The sequence operations were performed under the Platform Project for Supporting Drug Discovery and Life Science Research (Platform for Drug Discovery, Informatics,

and Structural Life Science) from the Japan Agency for Medical Research and Development (AMED) (to I.N. and S.I.). This study was also funded by a research grant from Fujita Health University (to S.I.), KAKENHI grants from the Japan Society for the Promotion of Science (JSPS) (#16K11118 to N.K.; #17KT0024 to H.Y.), PRESTO, JST (to H.Y.), Multidisciplinary Research Laboratory System of Osaka University (to H.Y.), and the Osaka University Program for the Support of Networking among Present and Future Researchers (to H.Y.).

AUTHOR CONTRIBUTIONS

S.I. conceptually designed this study and wrote the manuscript. S.I., N.K., and Y.Sh. performed and analyzed the biochemical experiments, including the chromatin fractionation. Y.Sa., M.U., and I.N. performed the NGS experiments. T.K. and I.N. designed and performed the bioinformatic analyses. H.Y. and M.A. performed and analyzed the HS-AFM experiments.

DECLARATION OF INTERESTS

The authors declare no competing interests.

EXPERIMENTAL PROCEDURES

Chromatin fractionation by using sedimentation velocity centrifugation

This chromatin fractionation technique is a modification of a method we established previously (Ishihara et al., 2010; Kotomura et al., 2015), and its schema is illustrated in Figure 1A. HepG2 cells (a human hepatoma cell line obtained from the RIKEN BRC in Japan) were used in this study. HepG2 cells were cultured in a minimum essential medium with α-modification supplemented with 10% fetal bovine serum. After washing with phosphate-buffered saline (PBS), 15 to 90 mg (wet weight) of HepG2 cells were collected into a microtube, and the concentration was adjusted to 15 mg/ml in PBS. For the crosslinking reaction, formalin (37% formaldehyde solution) was added to the cells at a final

concentration of 0.5%, and the cells were agitated at room temperature for 10 min. Following addition of glycine at a final concentration of 62.5 mM to quench the formaldehyde, the cells were washed twice with ice-cold PBS, solubilized with 250 to 500 μl of Tris-based SDS lysis buffer (TSB; 1% SDS, 50 mM Tris-HCl (pH 8.0), 10 mM EDTA, and a Complete Protease Inhibitor Cocktail (Roche)), and then fragmented with a Branson Sonifier 150 (at level "2" for 5 sec 6 times). After removal of the debris using a Vivaclear Mini column (Sartorius), the cell extract, including the chromatin fragments, was layered onto an 11 ml sucrose gradient (20–60%) in chromatin dilution buffer (CDB; 1.1% Triton X-100, 0.01% SDS, 16.7 mM Tris-HCl (pH 8.0), 1.2 mM EDTA, 167 mM NaCl, and a Complete Protease Inhibitor Cocktail (Roche)) in a polyallomer centrifugation tube (Beckman Coulter). The sample was then subjected to ultracentrifugation at 256,000 x g at 4°C for 16 hrs in a Beckman SW41Ti swing rotor. Following removal of the uppermost 1.8 ml volume, five 1.8 ml fractions were collected from the top to the bottom of the tube using a micropipette.

HS-AFM observation of fractionated chromatin

Chromatin was recovered from each fraction by immunoprecipitation with an anti-pan-histone H3 antibody (#ab1791, Abcam). Prior to the immunoprecipitation, 100 μg of the antibody was covalently conjugated to 17 mg of magnetic beads using a Dynabeads Antibody Coupling Kit (Thermo Fisher). The H3-conjugated beads (1.2 mg of beads) was mixed with each fraction, and the mixtures were agitated at 4°C overnight. After washing twice with CDB and then once with HE (50 mM Hepes (pH 7.6), 10 mM EDTA) at 4°C for 5 min each, the chromatin was eluted in 30 μl of Hepes-based SDS lysis buffer (HSB; 1% SDS, 50 mM Hepes (pH 7.6), 10 mM EDTA, and a Complete Protease Inhibitor Cocktail (Roche)). The HS-AFM observations were performed using a laboratory-built HS-AFM apparatus similar to a previously described AFM (Yamashita et al., 2013). The HS-AFM was equipped with small cantilevers (k = 0.1–0.2 N/m, f = 800–1200kHz in solution (Olympus)) and was operated in tapping mode. The AFM styli were placed on each cantilever by electron beam deposition. A sample stage made of quartz glass was placed on the z-scanner, and a 1.5 mm diameter mica disk was glued onto the sample stage. A freshly

cleaved mica surface was treated with 0.1% aminosilane for 90 s. After rinsing the surface with HE, 1.5 µl sample droplets of the chromatin preparations were placed on the mica surface and incubated for 3 min. All HS-AFM observations were performed under HE at room temperature. To estimate the sizes of the chromatin in each fraction, the diameters of the objects in the AFM images were analyzed using SPIP image analysis software (Image Metrology) and Origin (LightStone).

Preparation of DNA from fractionated chromatin

An aliquot of each fraction corresponding to the amount of sample from 3 mg of cells was used for preparation of DNA. Each aliquot was heated at 65°C overnight to reverse the crosslinking, and then successively treated with RNase A and proteinase K. Following phenol/chloroform extraction, DNA was recovered with 10 µg of glycogen by ethanol precipitation. Pellets were dissolved in 120 µl of TE (10 mM Tris (pH 7.5), 1 mM EDTA), treated with phenol/chloroform again, and then purified using a MinElute spin column (Qiagen). After elution with 30 µl of EB buffer (Qiagen), the DNA was quantified using a Quant-iT PicoGreen Kit (Thermo Fisher).

Analyses of the proteins in the fractionated chromatin

The remaining portions of the Fr-1 to Fr-3 fractions and the Fr-4 to Fr-5 fractions were diluted with 2 volumes and 3 volumes of CDB, respectively. To recover the proteins, 100% (w/v) TCA was added to the diluted fractions at a final concentration of 20%. The mixture was chilled on ice for 30 min and then centrifuged at 21,500 x g at 4°C for 20 min. After washing with ice-cold ethanol twice, the pellets were suspended in 130 µl (Fr-0), 110 µl (Fr-1), or 50 µl (Fr-2 to Fr-5) of TCA-pellet suspension buffer (TPS; 600 mM Tris (pH 8.8), 4% SDS, 8% glycerol, 0.01% bromophenol blue). To simultaneously solubilize the pellet and reverse the crosslinking, the suspension was heated at 65°C for 24 hrs. After centrifugation at 21,500 x g at 4°C for 10 min, the proteins were recovered in the supernatants. To observe the total protein in each fraction, the volumes of the protein preparations were adjusted with TPS among the fractions. Following treatment with 100 mM DTT at 100°C for 5 min, the total protein was

size-separated on an 8% polyacrylamide gel and stained with SYPRO Ruby (Lonza). When the contents of the protein preparation were analyzed by western blotting, the preparations were adjusted among the fractions with TPS based on the amount of DNA. Following treatment with dithiothreitol, the protein preparations were loaded onto a 10% (for histones) or 8% (for non-histone proteins) SDS-PAGE gel, ran, and then transferred to a nitrocellulose membrane (0.2 μm pore size). After blocking in 5% skim milk in Tris-buffered saline (TBS) with 0.1% Tween 20, the membranes were sequentially exposed to a primary antibody, a biotinylated secondary antibody, and streptavidin-conjugated alkaline phosphatase (GE Healthcare). They were then developed with a BCIP-NBT Solution Kit (Nacalai). To estimate the fractional distributions of the proteins, a standard curve for quantitation was calculated from the blot signals from serially diluted samples, whose intensities were measured using ImageJ. The primary and secondary antibodies are listed in Table S3.

Analyses of 5meC in the DNA from the fractionated chromatin

Two hundred ng of the DNA (adjusted to 30 μl) from each fraction was denatured by heating at 100°C for 5 min. After being immediately chilled on ice for 5 min, the DNA was spotted onto a nitrocellulose membrane (0.2 μm pore size) using a Bio-Dot Apparatus (Bio-Rad). After the membrane was baked at 80°C for 2 hrs, immunoblotting with an anti-5-methyl cytosine antibody (#ab1884, Abcam) was performed as described in the previous section.

Analyses of the DNA from the fractionated chromatin

For qPCR analyses, 500 pg (for the non-repeat sequences), 62.5 pg (for the L1 sequence), or 16.7 pg (for the *Alu* and α-satellite sequences) of the recovered DNA was used for a single reaction. To generate a standard curve, serially diluted human genomic DNA (0.76–12,500 pg; #D4642, Sigma-Aldrich) was utilized as previously described (Ishihara and Schwartz, 2011; Kotomura et al., 2015). The amount of each sequence was estimated from the respective PCR cycle threshold (Ct) value plotted on the standard curve. A 1:3 mixture of a QuantiFast SYBR Green PCR Kit (Qiagen) and a FastStart SYBR Green Master (Roche) in a real-time PCR machine (#7900HT, Applied Biosystems) was used

for the qPCR. The PCR primers are listed in Table S4. For preparation of an NGS sequence library of the DNA from the fractionated chromatin, 28 ng of the DNA in a Crimp-cap microTUBE (Covaris) was fragmented with an LE220 Focused-ultrasonicator (Covaris). The configuration of the ultrasonication process was as follows: temperature, 7ºC; duty factor, 30%; peak incident power, 450 W; cycles per burst, 200; and time, 190 sec. Following concentration via a DNA Clean & Concentrator-5 (Zymo Research), the fragmented DNA was converted to a sequence library using a KAPA Hyper Library Preparation Kit (KAPA Biosystems). To analyze transcripts in the HepG2 cells, 2 μg of total RNA was converted to a sequence library using a KAPA Stranded mRNA-seq Kit (KAPA Biosystems). These libraries were analyzed using a HiSeq 2500 sequencer (Illumina) with the following specifications: Read1, 50 cycles.

Bioinformatic analyses

The sequence reads were trimmed via the fastx_trimmer function of the FASTX-toolkit (version: 0.0.14), retaining the last 50 bps (parameter: “-l 50”). HISAT2 (version 2.0.4) was used to map the reads to the human hg38 genome with the default parameters. Samtools-0.1.19 fulfilled the requirement of HISAT2. The reads employed for our analyses were qualified via Samtools (version 1.3) with “samtools view -q 4” and were confirmed to not overlap in repetitive sequences of hg38 via intersectBed (bedtools v2.25.0) with option -v. The repetitive sequence data were obtained from the UCSC Genome Browser (https://genome.ucsc.edu/cgi-bin/hgTables). The transcription levels were evaluated as transcripts per kilobase million (TPM) using Sailfish (beta v0.10.0). Using this parameter, the transcription levels were categorized as follows: “Low”, log_10(TPM+1) < 0.15; “Mid”, 0.5 < log_10(TPM+1) <= 1.5; “High”, 2.0 < log_10(TPM+1). Ensemble76 reference data with the option “-p 20 -l SR -r” were employed for the transcript annotation. The read_distrobution.py Python script in RSeQC (version 2.6.4) was used to count the reads mapped to intergenic or intragenic regions, as shown in Figures S4 and S5. Hg38 genome annotation data (hg38_Gencode_V23.bed file in Sourceforge (https://sourceforge.net/p/rseqc/activity)) was used with the -r option of read_distrobution.py. Hierarchical clustering of the composition ratios of each

fraction was performed using the pvclust package (http://stat.sys.i.kyoto-u.ac.jp/prog/pvclust/) of the R program (with the bootstrap trial time equal to 1,000 (nboot = 1,000)). The read depth analyses were performed using bam2wig.py in RSeQC (version 2.6.4), specifying the wigsum as 8500000000 (-t 8500000000), skipping non-unique hits reads (-u), and fixing the chromosome sizes (-s “hg38 chromosome size file”). To obtain the Fr-5/Fr-1 scores for the entire genome, WiggleTools (https://github.com/Ensembl/WiggleTools) was used. First, the read depth scores were scaled by the amount of recovered DNA (“wiggletools scale” with Table S5), and 0.001 was added to each of the scores (“wiggletools offset 0.001”, to avoid substitution 0 for logarithm operation (Fr-5/Fr-1)). Next, division and logarithm operations (to obtain the Fr-5/Fr-1 scores) were performed (“wiggletools ratio” and “wiggletools log 2”). To obtain the fractional proportions of Fr-1 to Fr-5 at the TSSs and TESs, the ngs.plot.r script of the ngs.plot package (https://github.com/shenlab-sinai/ngsplot) was used. The data in Figure 6A were obtained from the results of ngs.plot.r with the option “-G hg38 -R ‘genebody’”. The genes that satisfied the requirement that the “read count per million mapped” values at the TSSs and TESs were larger than 0.05 (to avoid substitution 0 for logarithm operation (Fr-5 / Fr-1)) were used to extract the qualified data, as listed in Table S2, and to generate the scatter plots, along with the calculated approximation lines, presented in Figure 6B. Data (annotated to hg19) from a ChIP-Seq experiment for RNA Pol II in HepG2 cells were downloaded from the GEO database. The data were re-annotated to hg38 using the liftOver program (https://genome.ucsc.edu/cgi-bin/hgLiftOver). The protocols for producing Figures S8 and 7A were the same as the analyses used to produce Figures 6A and 6B, respectively.

REFERENCES

Adar, S., Hu, J., Lieb, J.D., and Sancar, A. (2016). Genome-wide kinetics of DNA excision repair in relation to chromatin state and mutagenesis. Proc. Natl. Acad. Sci. USA *113*, E2124–E2133.

Allis C.D., and Jenuwein, T. (2016). The molecular hallmarks of epigenetic control. Nat. Rev. Genet. *17*, 487–500.

Bell, O., Schwaiger, M., Oakeley, E.J., Lienert, F., Beisel, C., Stadler, M.B., and Schübeler, D. (2010). Accessibility of the Drosophila genome discriminates PcG repression, H4K16 acetylation and replication timing. Nat. Struct. Mol. Biol. *17*, 894–900.

Bell, O., Tiwari, V.K., Thomä, N.H., and Schübeler, D. (2011). Determinants and dynamics of genome accessibility. Nat. Rev. Genet. *12*, 554–564.

Bouchet-Marquis, C., Dubochet, J., and Fakan, S. (2006). Cryoelectron microscopy of vitrified sections: A new challenge for the analysis of functional nuclear architecture. Histochem. Cell Biol. *125*, 43–51.

Carone, B.R., Hung, J.H., Hainer, S.J., Chou, M.T., Carone, D.M., Weng, Z., Fazzio, T.G., and Rando, O.J. (2014). High-resolution mapping of chromatin packaging in mouse embryonic stem cells and sperm. Dev. Cell *30*, 11–22.

Chereji, R.V., Eriksson, P.R., Ocampo, J., Prajapati, H.K., and Clark, D.J. (2019) Accessibility of promoter DNA is not the primary determinant of chromatin-mediated gene regulation. Genome Res. *29*, in press.

Cockerill, P.N. (2011). Structure and function of active chromatin and DNase I hypersensitive sites. FEBS J. *278*, 2182–2210.

Dixon, J.R., Selvaraj, S., Yue, F., Kim, A., Li, Y., Shen, Y., Hu, M., Liu, J.S., and Ren, B. (2012). Topological domains in mammalian genomes identified by analysis of chromatin interactions. Nature *485*, 376–380.

Finch J.T., and Klug, A. (1976). Solenoidal model for superstructure in chromatin. Proc. Natl. Acad. Sci. USA *73*, 1897–1901.

Frenster, J.H., Allfrey, V.G., and Mirsky, A.E. (1963) Repressed and active chromatin insolated from interphase lymphocytes. Proc. Natl. Acad. Sci. USA *50*, 1026–1032.

Fussner, E., Strauss, M., Djuric, U., Li, R., Ahmed, K., Hart, M., Ellis, J., and

Bazett-Jones, D.P. (2012). Open and closed domains in the mouse genome are configured as 10-nm chromatin fibres. EMBO Rep. *13*, 992–996.

Gilbert, N., Boyle, S., Fiegler, H., Woodfine, K., Carter, N.P., and Bickmore, W.A. (2004). Chromatin architecture of the human genome. Cell *118*, 555–566.

Guertin, M.J., and Lis, J.T. (2013). Mechanisms by which transcription factors gain access to target sequence elements in chromatin. Curr. Opin. Genet. Dev. *23*, 116–123.

Hansen J.C. (2002). Conformational dynamics of the chromatin fiber in solution: determinants, mechanisms, and functions. Annu. Rev. Biophys. Biomol. Struct. *31*, 361-392.

Hihara, S., Pack, C.G., Kaizu, K., Tani, T., Hanafusa, T., Nozaki, T., Takemoto, S., Yoshimi, T., Yokota, H., Imamoto, N., et al. (2012). Local nucleosome dynamics facilitate chromatin accessibility in living mammalian cells. Cell Rep. *2*, 1645–1656.

Hsieh, T.H.S., Weiner, A., Lajoie, B., Dekker, J., Friedman, N., and Rando, O.J. (2015). Mapping nucleosome resolution chromosome folding in yeast by Micro-C. Cell *162*, 108–119.

Hughes A.L., and Rando, O.J. (2014). Mechanisms underlying nucleosome positioning in vivo. Annu. Rev. Biophys. *43*, 41–63.

Iglesias, N., and Moazed, D. (2017). Silencing repetitive DNA. eLife *6*, e29503.

Ishihara, S., Varma, R., and Schwartz, R.H. (2010). A new fractionation assay, based on the size of formaldehyde-crosslinked, mildly sheared chromatin, delineates the chromatin structure at promoter regions. Nucleic Acids Res. *38*, e124.

Ishihara S., and Schwartz, R.H. (2011). Two-step binding of transcription factors causes sequential chromatin structural changes at the activated IL-2 promoter. J. Immunol. *187*, 3292–3299.

Joti, Y., Hikima, T., Nishino, Y., Kamada, F., Hihara, S., Takata, H., Ishikawa, T.,

and Maeshima, K. (2012). Chromosomes without a 30-nm chromatin fiber. Nucleus *3*, 404–410.

Kalashnikova, A.A., Porter-Goff, M.E., Muthurajan, U.M., Luger, K., and Hansen, J.C. (2013). The role of the nucleosome acidic patch in modulating higher order chromatin structure. J. Royal Soc. Interface *10*, 20121022.

Kornberg, R.D. (1977). Structure of chromatin. Annu. Rev. Biochem. *46*, 931–954.

Kotomura, N., Harada, N., and Ishihara, S. (2015). The proportion of chromatin graded between closed and open states determines the level of transcripts derived from distinct promoters in the CYP19 gene. PLoS ONE *10*, e0128282.

Lai, B., Gao, W., Cui, K., Xie, W., Tang, Q., Jin, W., Hu, G., Ni, B., and Zhao, K. (2018). Principles of nucleosome organization revealed by single-cell micrococcal nuclease sequencing. Nature *562*, 281–285.

Lever, M.A., Th'ng, J.P.H., Sun, X., Hendzel, M.J. (2000). Rapid exchange of histone H1.1 on chromatin in living human cells. Nature *408*, 873–876.

Lieberman-Aiden, E., Van Berkum, N.L., Williams, L., Imakaev, M., Ragoczy, T., Telling, A., Amit, I., Lajoie, B.R., Sabo, P.J., Dorschner, M.O., et al. (2009). Comprehensive mapping of long-range interactions reveals folding principles of the human genome. Science *326*, 289–294.

Luger, K., Mäder, A.W., Richmond, R.K., Sargent, D.F., and Richmond, T.J. (1997). Crystal structure of the nucleosome core particle at 2.8 Å resolution. Nature *389*, 251–260.

Machida, S., Takizawa, Y., Ishimaru, M., Sugita, Y., Sekine, S., Nakayama, J.I., Wolf, M., and Kurumizaka, H. (2018) Structural Basis of Heterochromatin Formation by Human HP1. Mol. Cell *69*, 385-397.

Maeshima, K., Kaizu, K., Tamura, S., Nozaki, T., Kokubo, T., and Takahashi, K. (2015). The physical size of transcription factors is key to transcriptional regulation in chromatin domains. J. Phys. Condens. Matter *27*, 064116.

Maeshima, K., Ide, S., and Babokhov, M. (2019). Dynamic chromatin organization without the 30-nm fiber. Curr. Opin. Cell Biol. *58*, 95-104.

Marand, A.P., Jansky, S.H., Zhao, H., Leisner, C.P., Zhu, X., Zeng, Z., Crisovan, E., Newton, L., Hamernik, A.J. Veilleux, R.E., et al. (2017) Meiotic crossovers are associated with open chromatin and enriched with Stowaway transposons in potato. Genome Biol. *18*, 203.

Miotto, B., Ji, Z., and Struhl, K. (2016). Selectivity of ORC binding sites and the relation to replication timing, fragile sites, and deletions in cancers. Proc. Natl. Acad. Sci. USA *113*, E4810–E4819.

Misteli, T., Gunjan, A., Hock, R., Bustin, M., Brown, D.T. (2000). Dynamic binding of histone H1 to chromatin in living cells. Nature *408*, 877–881.

Nora, E.P., Lajoie, B.R., Schulz, E.G., Giorgetti, L., Okamoto, I., Servant, N., Piolot, T., van Berkum, N.L., Meisig, J., Sedat, J., et al. (2012). Spatial partitioning of the regulatory landscape of the X-inactivation centre. Nature *485*, 381-385.

Nozaki, T., Kaizu, K., Pack, C.G., Tamura, S., Tani, T., Hihara, S., Nagai, T., Takahashi, K., and Maeshima, K. (2013). Flexible and dynamic nucleosome fiber in living mammalian cells. Nucleus *4*, 349–356.

Nozaki, T., Imai, R., Tanbo, M., Nagashima, R., Tamura, S., Tani. T., Joti, Y., Tomita, M., Hibino, K., Kanemaki, M.T., et al. (2017). Dynamic organization of chromatin domains revealed by super-resolution live-cell imaging. Mol. Cell *67*, 282-293.

Ricci, M.A., Manzo, C., García-Parajo, M.F., Lakadamyali, M., and Cosma, M.P. (2015). Chromatin fibers are formed by heterogeneous groups of nucleosomes in vivo. Cell *160*, 1145–1158.

Rodgers-Melnick, E., Vera, D.L., Bass, H.W., and Buckler, E.S. (2016). Open chromatin reveals the functional maize genome. Proc. Natl. Acad. Sci. USA *113*, E3177–E3184.

Saksouk, N., Simboeck, E., and Déjardin, J. (2015). Constitutive heterochromatin formation and transcription in mammals. Epigenet. Chromatin *8*, 3.

Schones, D.E., Cui, K., Cuddapah, S., Roh, T.Y., Barski, A., Wang, Z., Wei, G., and Zhao, K. (2008). Dynamic regulation of nucleosome positioning in the human genome, Cell *132*, 887–898.

Schwartz, U., Németh, A., Diermeier, S., Exler, J.H., Hansch, S., Maldonado, R., Heizinger, L. Merkl, R., and Längst, G. (2019). Characterizing the nuclease accessibility of DNA in human cells to map higher order structures of chromatin. Nucleic Acids Res. *47*, 1239-1254.

Sexton, T., Yaffe, E., Kenigsberg, E., Bantignies, F., Leblanc, B., Hoichman, M., Parrinello, H., Tanay, A., and Cavalli, G. (2012). Three-dimensional folding and functional organization principles of the Drosophila genome. Cell *148*, 458-472.

Small, E.C., Xi, L., Wang, J.P., Widom, J., and Licht, J.D. (2014). Single-cell nucleosome mapping reveals the molecular basis of gene expression heterogeneity, Proc. Natl. Acad. Sci. USA *111*, E2462–E2471.

Teif, V.B., Vainshtein, Y., Caudron-Herger, M., Mallm, J.P., Marth, C., Höfer, T., and Rippe, K. (2012). Genome-wide nucleosome positioning during embryonic stem cell development. Nat. Struct. Mol. Biol. *19*, 1185–1192.

Tsompana M., and Buck, M.J. (2014). Chromatin accessibility: A window into the genome. Epigenet. Chromatin *7*, 33.

Voong, L.N., Xi, L., Sebeson, A.C., Xiong, B., Wang, J.P., and Wang, X. (2016). Insights into nucleosome organization in mouse embryonic stem cells through chemical mapping. Cell *167*, 1555–1570.

Voong, L.N., Xi, L., Wang, J.P., and Wang, X. (2017). Genome-wide mapping of the nucleosome landscape by micrococcal nuclease and chemical mapping. Trends Genet. *33*, 495–507.

White, A.E., Hieb, A.R., and Luger, K. (2016). A quantitative investigation of

linker histone interactions with nucleosomes and chromatin. Sci. Rep. *6*, 19122.

Wood, K.H., and Zhou, Z. (2016). Emerging molecular and biological functions of MBD2, a reader of DNA methylation. Front. Genet. *7*, 93.

Woodcock, C.L.F., Frado, L.L.Y., and Rattner, J.B. (1984) The higher-order structure of chromatin: evidence for a helical ribbon arrangement. J. Cell Biol. *99*, 42-52.

Woodcock, C.L., and Ghosh, R.P. (2010). Chromatin higher-order structure and dynamics. Cold Spring Harb. Perspect. Biol. *2*, a000596.

Yamashita, H., Inoue, K., Shibata, M., Uchihashi, T., Sasaki, J., Kandori, H., and Ando, T. (2013). Role of trimer–trimer interaction of bacteriorhodopsin studied by optical spectroscopy and high-speed atomic force microscopy. J. Struct. Biol. *184*, 2-11.